VSP

Journal of Adhesion Science and Technology 23 (2009) 361–380

Journal of ADHESION SCIENCE and TECHNOLOGY
www.brill.nl/jast

Tunability of the Adhesion of Water Drops on a Superhydrophobic Paper Surface *via* Selective Plasma Etching

Balamurali Balu, Jong Suk Kim, Victor Breedveld and Dennis W. Hess *

School of Chemical and Biomolecular Engineering, Georgia Institute of Technology, 311 Ferst Drive, Atlanta, GA 30332-0100, USA

Received in final form 20 October 2008

Abstract

We report the fabrication of a sticky superhydrophobic paper surface with extremely high contact angle hysteresis: advancing contact angle ∼150° (superhydrophobic) and receding contact angle ∼10° (superhydrophilic). In addition, we report the controlled tunability of the contact angle hysteresis from $149.8 \pm 5.8°$ to $3.5 \pm 1.1°$, while maintaining superhydrophobicity, as defined through an advancing contact angle above 150°. The hysteresis was tuned through the controlled fabrication of nano-scale features on the paper fibers *via* selective plasma etching. The variations in contact angle hysteresis are attributed to a transition of the liquid–surface interaction from a Wenzel state to a Cassie state on the nano-scale, while maintaining a Cassie state on the micro-scale. Superhydrophobic cellulosic surfaces with tunable stickiness or adhesion have potential applications in the control of aqueous drop mobility and the transfer of drops on inexpensive, renewable substrates.

Keywords

Sticky, superhydrophobic, superhydrophilic, paper, cellulose, tunability, hysteresis, plasma, etching

1. Introduction

In 1805 Young [1] proposed a relationship between the forces acting at an interface between a liquid and a solid. At that time, he did not formulate the equation that now bears his name, but expressed his ideas in words: '... for each combination of a solid and a fluid, there is an appropriate angle of contact between the surfaces of the fluid, exposed to the air, and to the solid...'. With several assumptions, Gibbs

* To whom correspondence should be addressed. Tel.: (404) 894-5922; Fax: (404) 894-2866; e-mail: dennis.hess@chbe.gatech.edu

 DOI:10.1163/156856108X383547

later reformulated this hypothesis into the equation that has been widely accepted as Young's equation [2]:

$$\gamma_{SV} = \gamma_{SL} + \gamma_{LV} \cos\theta. \tag{1}$$

One of the important assumptions in the Young's equation is that the energy of the system reaches a global minimum surrounded by infinitesimally close non-equilibrium states in the energy landscape [2]. However, this scenario is not realistic for real surfaces because of the presence of physical and chemical heterogeneities, which give rise to the presence of local minima surrounding the global energy minimum. As a result, most real surfaces exhibit a variety of contact angles for a particular solid–liquid–vapor combination, rather than a unique '... appropriate angle of contact ...' as proposed by Young. Although Wenzel [3, 4] and Cassie [5] modified Young's equation for physical and chemical heterogeneities, respectively, the inherent assumption of the system being in the global energetic minimum still exists. Indeed, Johnson and Dettre [2, 6–8] described the limitations that may be encountered when applying Young's hypothesis, as well as other mathematical formulations (e.g., Wenzel's and Cassie's equations), to real surfaces.

More than one hundred years after Young's essay, the first observation of multiple contact angle (CA) values for the same solid–liquid–vapor system was reported [9]. Despite the observation of various CA values, well-defined maximum and minimum contact angles could be identified and the term 'contact angle hysteresis' was introduced to designate the difference between these two contact angles [9]. The maximum and minimum contact angles were later termed advancing and receding contact angles, respectively. In order to properly characterize the wetting properties of all substrates, it is critical to take contact angle hysteresis into account.

The presence of hysteresis becomes critical with regards to superhydrophobic surfaces (as defined by a static or advancing CA $> 150°$). Superhydrophobic surfaces are often correlated with water repellency, but the presence of hysteresis on a superhydrophobic surface might disguise such behavior as it causes water drops to stick to the surface. Water droplets easily roll-off superhydrophobic surfaces if the CA hysteresis is below $\sim 10°$, depending on the size of the drops. For larger CA hysteresis, water droplets tend to stick even to superhydrophobic substrates (advancing CA greater than $\sim 150°$). As a result, the functional classification of superhydrophobic substrates depends on CA hysteresis. Indeed, approximately 10 years ago it was noted that for the characterization of (super)hydrophobic substrates it is necessary to determine both the advancing and receding CAs (i.e., hysteresis) [10, 11]. Over the past few decades various names have been used to describe surfaces with static or advancing CA larger than 150° (Table 1).

A recent review on superhydrophobicity indicates that only surfaces with both an advancing CA greater than 150° and CA hysteresis less than 10° should be termed superhydrophobic [31]; however, this strict definition excludes surfaces with CA hysteresis $> 10°$, which exhibit interesting behavior. In a previous paper we described superhydrophobic substrates with vastly different CA hys-

Table 1.
Terminology used to describe superhydrophobic surfaces

Static or advancing CA	CA hysteresis	Terms used to describe superhydrophobicity
>150°	<10°	Absolutely hydrophobic [12], water-repellant [5], ultrahydrophobic [10, 13] and superhydrophobic [14–16]
>150°	>10°	Super water-repellent [17], highly hydrophobic [18], water repulsive [19, 20] and superhydrophobic [21–24]
>150°	Not reported	Ultra water-repellant [25–27], ultrahydrophobic [28, 29] and superhydrophobic [15, 30]

teresis values and, to avoid confusion, proposed simple terms to describe two generic forms of superhydrophobicity [32]: roll-off superhydrophobicity (CA > 150° and CA hysteresis < 10°) and sticky superhydrophobicity (CA > 150° and CA hysteresis > 10°).

'Roll-off' superhydrophobic surfaces have been extensively investigated in reference to self-cleaning substrates, often referred to as surfaces mimicking the lotus effect. By comparison, much less information has been reported on the fabrication of 'sticky' superhydrophobic surfaces. So-called sticky superhydrophobic surfaces possess a unique combination of high adhesion force and small liquid–solid contact area. The mobility of water droplets on such sticky superhydrophobic surfaces can, in principle, be manipulated by tuning the adhesion force, which may enable novel applications in the chemical and biomedical arenas. Examples are the development of 'tweezers' for liquid drops, controlled mobility of liquid drops on inclined surfaces, selective permeability in membranes, as well as proteomics and genomics microarrays.

To our knowledge, the first sticky superhydrophobic surface was fabricated by Johnson and Dettre [7], and displayed an advancing CA = ∼160° with CA hysteresis = ∼100°; this discovery has gone largely unnoticed, because of the lack of knowledge about possible applications at that time. More recently, a number of publications have appeared that report superhydrophobic surfaces with high hysteresis values [12, 13, 17, 21, 32]. In addition, a number of publications have reported superhydrophobic surfaces that are able to immobilize water droplets up to various tilt angles [18, 21, 33–37], without actually reporting CA hysteresis values. Finally, several publications have reported the stickiness of a superhydrophobic surface in terms of the adhesion force [22–24, 38]. Because the adhesion force of a droplet on a surface depends on factors such as surface inclination and drop size [34, 39–42], CA hysteresis is a more appropriate parameter to enable comparison of surface characteristics.

We are not aware of reports of the fabrication of superhydrophobic surfaces that can be tuned from sticky to roll-off by simply controlling the receding contact

angles from superhydrophilic ($<10°$) to superhydrophobic ($>150°$). The publications on sticky superhydrophobic surfaces referenced in the above paragraph suggest that droplets can be removed completely from the sticky substrate if the applied force is sufficiently large. However, if the receding contact angle is superhydrophilic ($<10°$), the droplet forms a bridge and breaks during its separation from the sticky superhydro phobic surface. Reports to date have indicated only a small window for hysteresis tunability, with the maximum hysteresis less than 100° [7, 12, 13, 21, 33].

In this paper, we report the fabrication of a sticky superhydrophobic surface with superhydrophobic advancing CA and superhydrophilic receding CA on cellulosic materials (e.g., paper), resulting in a high CA hysteresis value of $149.8 \pm 5.8°$. In addition, we report methods for tuning this hysteresis (i.e., stickiness) from $149.8 \pm 5.8°$ to $3.5 \pm 1.1°$. We achieve this by controlling the formation of physical heterogeneities (roughness) of the paper fibers by selective etching of the amorphous cellulose domains in an oxygen plasma. The low surface energy of these etched paper surfaces is obtained by depositing a thin film of pentafluoroethane (PFE) from the plasma environment. The fact that these substrates are based on cellulosic paper, a biodegradable, inexpensive, flexible, biopolymer, widens its potential commercial interests.

2. Experimental

2.1. Handsheet Formation

Commercial copy paper contains filler particles and other additives to enhance its physical and optical properties. In order to initially avoid the interaction of these particles with the surface modification techniques employed, we used control samples, generally referred to as handsheets, which were prepared according to TAPPI standardized method T205 sp-02 using southern hardwood kraft (Alabama River Pulp Co.) and southern softwood kraft (North Carolina International Paper). The handsheets were fabricated to ensure that the most relevant properties of the handsheets were in the same range as those of commercial copy paper: basis weight (66.68 ± 2.68 g/m^2), thickness (105.59 ± 4.86 μm) and roughness (amplitude $R_a = 6.17 \pm 0.24$ μm). Four types of substrates were prepared with different fiber combinations and drying methods as shown in Table 2.

2.2. Plasma Etching/Deposition

The details of the parallel plate rf (13.56 MHz) plasma reactor configuration and operational procedures can be found elsewhere [32]. The experimental conditions for oxygen etching to create appropriate roughness of the cellulose fibers and subsequent deposition of a fluorocarbon film from pentafluoroethane (PFE) monomer are listed in Table 3.

Table 2.
Method of drying and fiber type of handsheets

Handsheet designation	Method of drying	Fiber type
HS-OD	Overnight drying	50% hardwood–50% softwood
H	Rapid drying	100% hardwood
S	Rapid drying	100% softwood
HS	Rapid drying	50% hardwood–50% softwood

Table 3.
Plasma reactor parameters for the etching of and deposition on handsheets

Parameters	Etching	Deposition
Gas	Oxygen	Pentafluoroethane (PFE) and Argon
Flow rate	75 sccm	20 sccm (PFE) and 75 sccm (Argon)
Temperature	110°C	110°C
Pressure	0.55 Torr	1 Torr
Power	10 W	120 W

2.3. XPS

XPS spectra were obtained using a PHI model 1600 spectrometer. Further details of this instrument can be found elsewhere [43].

2.4. ATR–FT-IR

FT-IR spectra were obtained from a Bruker Equinox 55 FT-IR spectrometer, equipped with a nitrogen cooled MCT detector. Further details of this equipment can be found elsewhere [44]. A thin strip of the substrate (0.76 cm × 6.35 cm) was cut and pressed against a ZnSe ATR crystal using a flat metal strip. The pressure on the sample was controlled by a set screw and kept approximately constant for all the samples.

2.5. SEM

SEM micrographs were obtained (LEO 1530, Carl Zeiss SMT Inc., Peabody, MA) at an operation voltage of 10 kV. Substrates were sputter coated (EMS 350; Electron Microscopy Sciences, Hatfield, PA) with a thin film of gold (15 nm) prior to SEM studies.

2.6. Water Contact Angle Measurements

The handsheet was placed on a translation stage, a 4 μl drop suspended from a needle was brought into contact, and the stage was moved in the x-direction (left to right) [9]. The CAs on the advancing and receding sides of the drop were measured.

The advantage of this dynamic method is that it scans a large substrate area and thus yields better statistically averaged values of CA, especially for heterogeneous substrates like paper. One of the disadvantages of this method is that receding CA values of less than 10° cannot be measured, because the drop can break apart while being dragged on the surface [9]. For our most sticky substrates, the receding CA was in this range and the breakup of drops was observed. In these cases, the standard volume increment/decrement method for measuring advancing and receding CAs was used. The droplet volume was increased from 4 μl to 12 μl in increments of 4 μl to measure the advancing CA. Thereafter, small decrements of 0.17 μl were used to measure the receding CA.

3. Results and Discussion

Before measuring the wetting properties of our modified substrates, we subjected the substrates to basic physicochemical tests to determine their physical and chemical properties after oxygen etching and PFE deposition in the plasma reactor.

3.1. XPS

Cellulose fiber surfaces were characterized after etching and deposition of PFE layers by XPS analysis. Cellulose molecules $(C_6H_{10}O_5)_n$ are essentially polymer chains of β-d-glucose residues covalently coupled *via* glucosidal linkages [45, 46]. Consistent with this molecular structure, the XPS survey spectrum of the cellulose handsheet (Fig. 1a) displays two intense peaks assigned to O_{1s} (oxygen) and C_{1s} (carbon). Moreover, the theoretical O/C ratio of cellulose (0.83) correlates well with the ratio of 0.84 ± 0.01 determined by XPS, which indicates that the fabricated handsheets do not contain fillers or other impurities found in commercial paper, and therefore that the handsheets can be used as model substrates for cellulose fibers. Indeed, previous work in our laboratory has demonstrated the similarity between the superhydrophobic character of treated handsheets and analogously treated commercial copy paper [32].

The primary etchant species formed in an oxygen plasma are oxygen radicals (O^*) and oxygen atoms ($O^\bullet$) [32], which etch cellulosic materials (P) *via* the following reaction pathways [32, 47]:

$$P + O^* \rightarrow P^* + OH \tag{2}$$

$$P^* + O^\bullet \rightarrow P'O + CO + CO_2 \tag{3}$$

The XPS survey spectra of the etched handsheets (data not shown) did not detect the presence of new elements, indicating that no impurities were added to the handsheet surface during plasma etching. Table 4 shows the %carbon, %oxygen and O/C ratio of the handsheets etched in the oxygen plasma for different etching times. The O/C ratio increases as a function of etching time, consistent with continued oxidation, surface conversion and etching of cellulose by oxygen species.

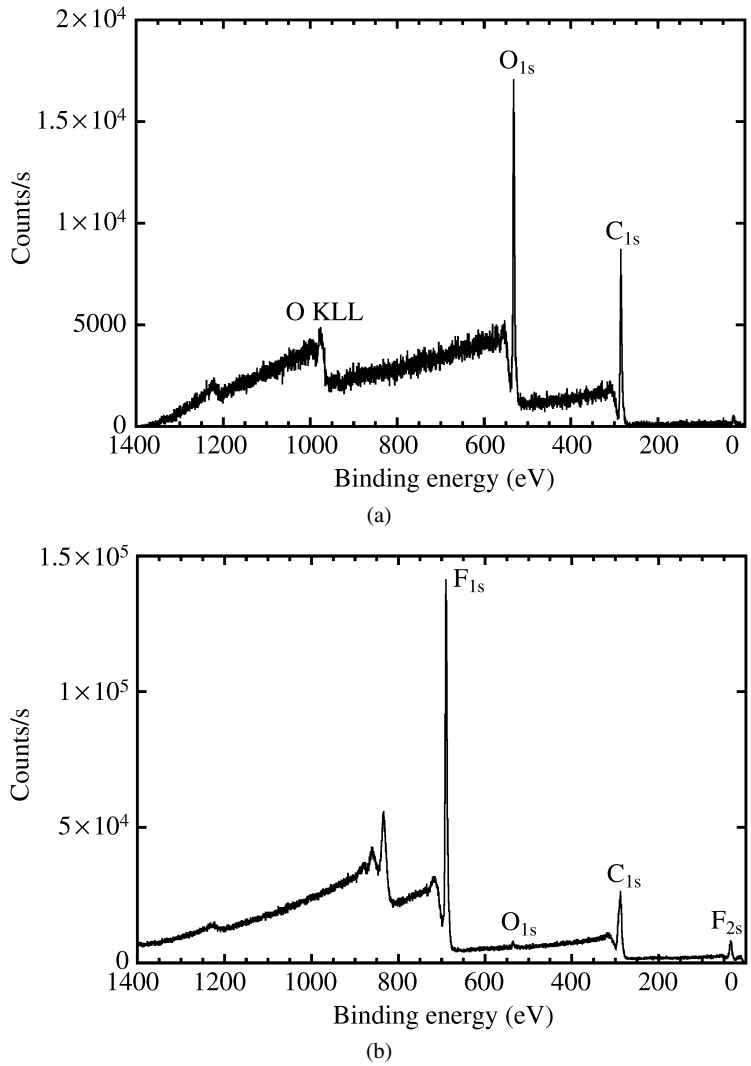

Figure 1. XPS survey spectra of untreated handsheet (HS-OD) (a) and PFE film on Si wafer (b).

Table 4.
Atomic percentages of carbon (C) and oxygen (O), and O/C ratio with respect to etching time

Etching time (min)	%C	%O	O/C ratio
0	54.38 ± 0.20	45.62 ± 0.20	0.84 ± 0.01
10	49.28 ± 2.27	50.72 ± 2.27	1.03 ± 0.10
15	48.05 ± 0.81	51.95 ± 0.81	1.08 ± 0.04
30	44.12 ± 1.20	55.88 ± 1.20	1.27 ± 0.06

An XPS survey spectrum after deposition of the fluorocarbon film on Si wafer from the PFE precursor is shown in Fig. 1b. The hydrophobic nature of the film is evident from the two intense fluorine peaks (F_{1s} and F_{2s}) and a reduction in the intensity of the oxygen peak. High resolution C_{1s} spectra of the PFE film revealed the highly cross-linked nature of the film (F/C ratio ∼1.1) and the presence of various hydrophobic fluorinated moieties (CF_x) [43, 48].

3.2. ATR–FT-IR

XPS is a surface analysis technique with a probing depth of electrons ranging from 8 to 10 nm. To study the chemical nature of the PFE–cellulose structure in more detail, FT-IR spectra of untreated and PFE-deposited handsheets (HS-OD) were obtained with a penetration depth of 1.2 μm at 900 cm^{-1} [44]. Figure 2a and 2b shows the FT-IR spectra of the untreated and PFE-coated handsheets (film thickness ∼400 nm). Spectrum of the untreated handsheet correlates well with the FT-IR spectrum of cellulose surfaces reported previously [49, 50]. With the deposition of the PFE film on the handsheet (Fig. 2b) there is suppression of cellulose absorption bands: 3348 cm^{-1} (O–H stretch), 1336 cm^{-1} (O–H in-plane deformation), 2902 cm^{-1} (C–H stretch), 1430 cm^{-1} (C–H deformation, asymmetric) and 1059 cm^{-1} (C–O stretch), which indicates a lower level of oxygen and hydrogen present on the surface. The presence of the new absorption bands at 1200 cm^{-1} (CF_x stretch) and 1700 cm^{-1} (unsaturated fluorocarbon bonds) confirms the presence of a fluorocarbon film. Thus, the spectrum of the handsheet after PFE deposition exhibits features of both an untreated handsheet (Fig. 2a) and a PFE film [43]. This supports the hypothesis that plasma deposition does not significantly affect the

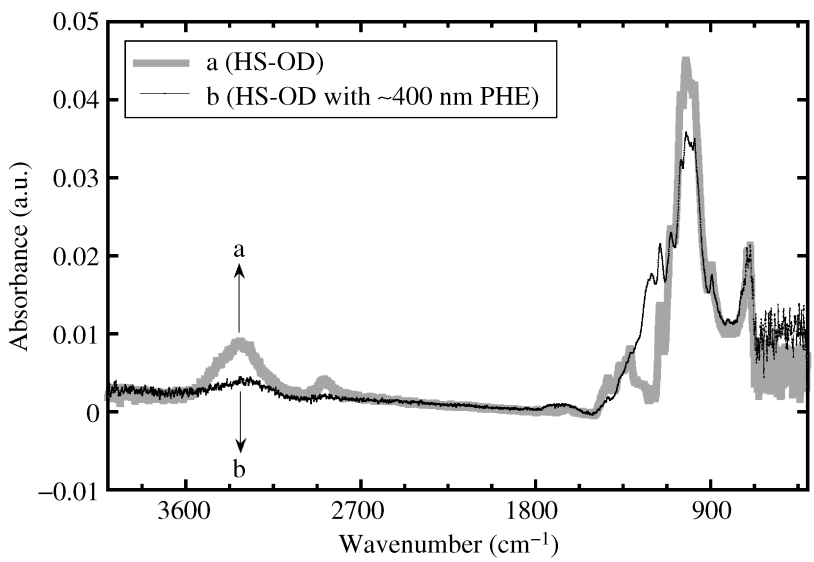

Figure 2. ATR–FT-IR survey spectra of untreated (a) and PFE-coated (∼400 nm film) handsheets (HS-OD) (b).

chemical nature of the cellulose fibers, although the PFE is chemically bonded to the cellulose surface.

Paper is a complex porous substrate containing tortuous pores with a wide pore size distribution. Although plasma processing of paper substrates is widely referred to as a surface modification process, one might expect that there will be some penetration and reaction of plasma species into the paper bulk [51]. Preliminary SEM images of PFE-coated handsheets after the creation of cross-sections *via* focused ion beam etching show that the PFE deposition occurs primarily on the surface of the handsheet in spite of its porosity.

3.3. Fabrication of Sticky Superhydrophobic Paper Surfaces

Handsheets (HS-OD, H, S and HS) were exposed to PFE deposition for 2 min (no etching) which generated a film thickness of ∼100 nm. Contact angle measurements were performed; Table 5 shows the advancing CA, receding CA and CA hysteresis results.

All four substrates exhibit extremely high hysteresis values, with advancing CAs nearly in the superhydrophobic regime and receding CAs in the superhydrophilic regime. Selected images of the advancing and receding CA measurements are shown in Fig. 3. It is evident from the image sequence in Fig. 3 that during the receding period, the apparent solid–liquid contact area did not decrease indicative of the extreme stickiness of the water drop to the surface.

3.4. Tunability of the Stickiness

Recently, we reported the fabrication of 'sticky' and 'roll-off' superhydrophobic paper surfaces [32]. The sticky superhydrophobic surface we reported had a CA hysteresis of $79.1 \pm 15.8°$, far less than the CA hysteresis values shown in Table 5. After obtaining the extremely high hysteresis values for the sticky substrates in our current study, we systematically varied the hysteresis in order to control the stickiness of the surfaces toward water drops. That is, we expected that the stickiness (i.e., CA hysteresis) could be manipulated by controlling the physical heterogeneity of the paper surfaces. This was achieved by selectively etching the amorphous portions of the cellulose fibers by selective oxygen etching [32]. To investigate this process, handsheets (HS-OD) were etched in an oxygen plasma for different du-

Table 5.
Contact angle measurements on sticky superhydrophobic paper surfaces

Handsheet	Advancing CA (°)	Receding CA (°)	CA hysteresis (°)
HS-OD	155.6 ± 4.0	8.4 ± 6.8	147.2 ± 6.8
H	154.3 ± 1.9	12.5 ± 5.0	141.8 ± 5.0
S	149.0 ± 2.5	8.5 ± 5.0	140.4 ± 5.0
HS	159.4 ± 7.7	9.7 ± 5.8	149.8 ± 5.8

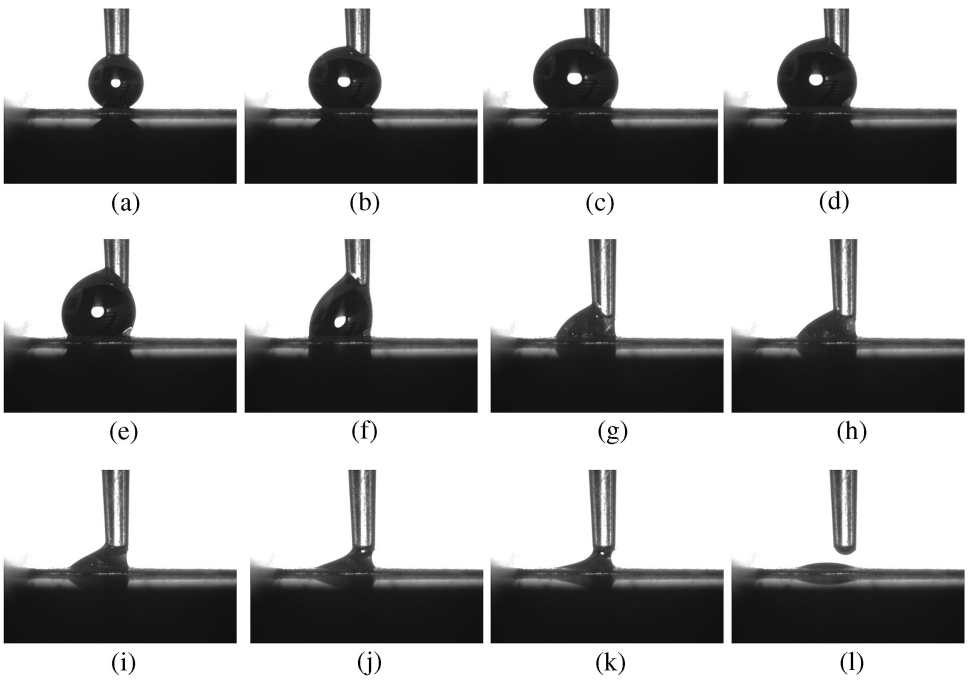

Figure 3. Selected images of advancing (a–c) and receding contact angle (d–l) measurements on a sticky superhydrophobic handsheet surface (S).

rations (0–60 min). Film deposition was then performed onto the handsheets for 2 and 15 min to form a thin film of PFE.

Figure 4 shows advancing CAs, receding CAs and CA hysteresis for the handsheets (HS-OD) processed with different etching times. It is evident from Fig. 4 that while the advancing CA is in the superhydrophobic regime for all samples ($>150°$), the receding CA increases from a superhydrophilic value of $8.4 \pm 6.8°$ to superhydrophobic value of $155.4 \pm 1.6°$. This smooth transition of the receding CA results in tunable CA hysteresis values from $147.2 \pm 6.8°$ (sticky) to $7.6 \pm 1.6°$ (roll-off). Controlling the oxygen etching times thus enables the generation of paper surfaces with various levels of stickiness.

SEM images of the handsheets (HS-OD) for selected etch times and 2 min PFE deposition are shown in Fig. 5a (high magnification) and 5b (low magnification). On the nano-scale (Fig. 5a), we see that as oxygen etching proceeds, the fiber surfaces are roughened due to the formation of small nano-scale features. After 10 min etching, the formation of mushroom-like features is apparent. The feature spacing increases with prolonged etching (30 min) and, after 60 min etching, the mushroom-like features have disappeared; at this point the nano-scale roughness consists of solid ridges. On the micro-scale (Fig. 5b), the number density of fibers on the surface decreases with etching time, which results in enhanced micro-scale roughness. The oxygen plasma apparently etches away the soft fiber

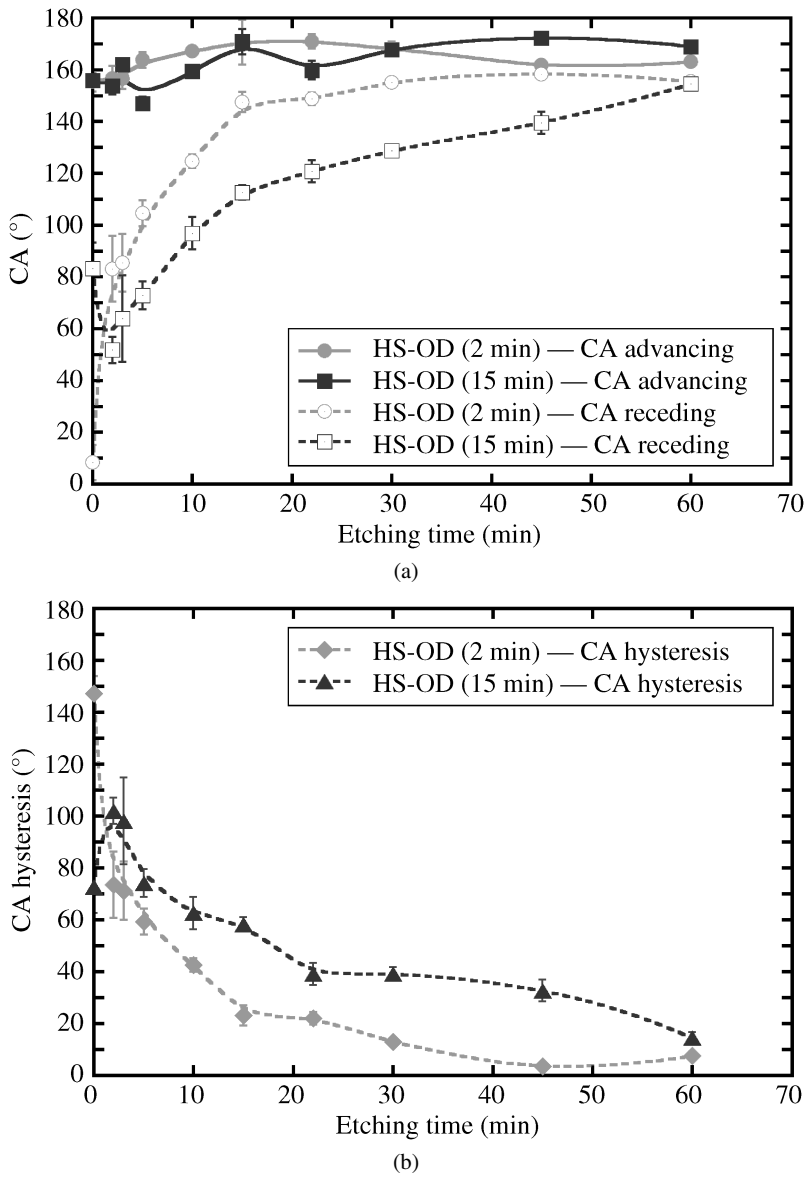

Figure 4. (a) Plot of advancing CA and receding CA of handsheets (HS-OD) with respect to oxygen plasma etching time for 2 min and 15 min PFE depositions. (b) Plot of CA hysteresis of handsheets (HS-OD) with respect to oxygen plasma etching time for 2 min and 15 min PFE depositions.

dust and primary layers of fibers. It is evident from the figures that oxygen etching roughens the handsheet surface on two separate length scales; the extent of both roughness scales qualitatively increases with etching time, at least up to 30 min etching.

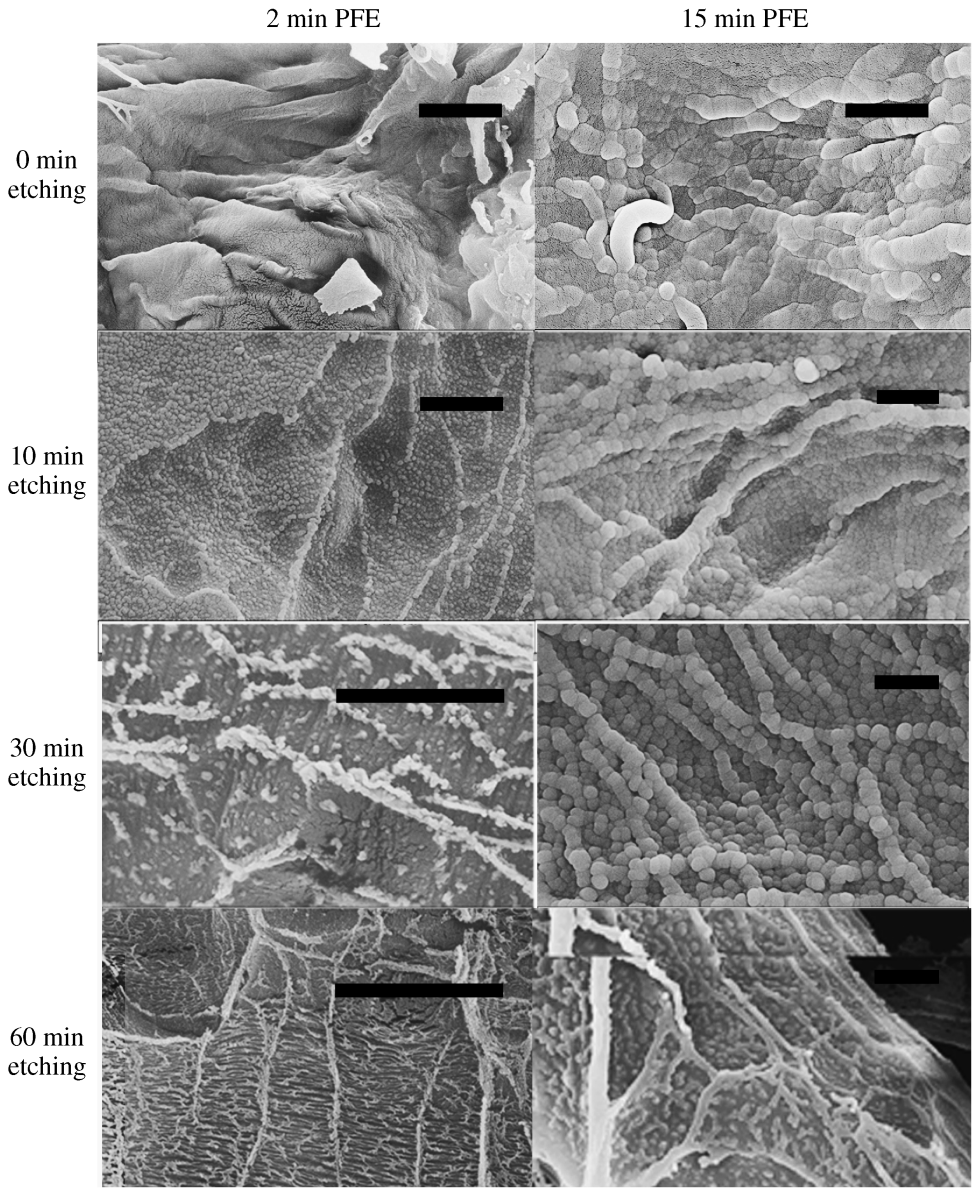

(a)

Figure 5. (a) High-magnification images of the HS-OD (with 2 min PFE deposition) and HS-OD (with 15 min PFE deposition) for 0, 10, 30 and 60 min etching times. The scale bars correspond to 2 μm.

3.5. Mechanism for Tunability of the Stickiness

The interactions of a liquid drop with a physically heterogeneous (rough) solid surface can be explained by two classic equations: Wenzel [3] and Cassie [5]. When

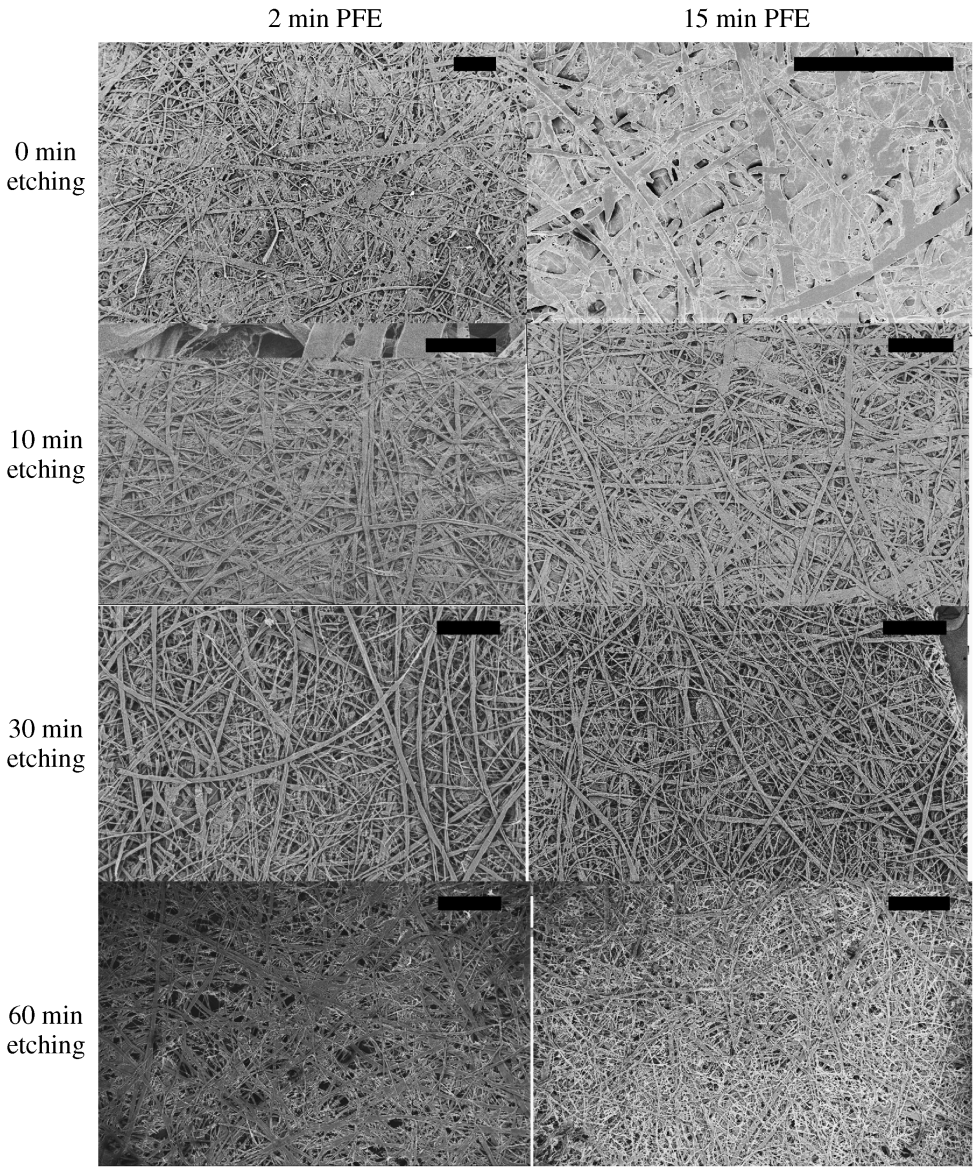

(b)

Figure 5. (Continued.) (b) Low-magnification images of the HS-OD (with 2 min PFE deposition) and HS-OD (with 15 min PFE deposition) for 0, 10, 30 and 60 min etching times. The scale bars correspond to 400 μm.

the liquid penetrates into the rough grooves of the surface, the apparent contact angle made by the liquid drop with the surface was described by Wenzel [3] as follows:

$$\cos\theta = r\cos\theta_y, \tag{4}$$

where r is the ratio between the actual surface area to the geometric (projected) surface area ($r > 1$ for a rough surface with complete liquid–substrate contact), θ and θ_y are the apparent and Young's contact angles of the surface, respectively.

On the other hand, when the liquid does not completely penetrate into the solid grooves, leaving air voids at the apparent solid–liquid interface, the apparent contact angle of the liquid drop with the surface was described by Cassie and Baxter [5] as follows:

$$\cos\theta = f\cos\theta_y - (1 - f), \tag{5}$$

where f is the solid–liquid area fraction, θ and θ_y are, respectively, the apparent and Young's contact angles of the surface. Johnson and Dettre [2, 7] later combined these two equations (4) and (5) to model the transition from a Wenzel-type wetting to a Cassie-type wetting as a function of roughness. They concluded that for a hydrophobic surface, the CA hysteresis increases with roughness if the wetting is governed by the Wenzel state. On the other hand, the CA hysteresis decreases with roughness if the wetting is governed by the Cassie state.

Paper is a porous substrate consisting of many tortuous pores formed by the complex network of cellulose fibers. When a thin PFE film is deposited (∼100 nm), only the individual fibers are coated and the porosity and the roughness of the paper substrate are unchanged [48]. Therefore, even without the presence of roughness created by oxygen etching, an inherent micro-scale roughness of the paper surface results from the network of fibers and the porosity of the paper; this causes the interaction of a liquid drop with paper to be in the Cassie regime. From Fig. 4 it is evident that the hysteresis of the handsheets (HS-OD) decreases with respect to the etching time, which suggests that the etched handsheets are also in the Cassie regime.

The static CA for a smooth PFE film deposited on a silicon wafer is approximately 105°. After a continuous PFE film covers the fiber surface, the surface chemistry of the fiber becomes identical to that of a PFE film (concluded from the XPS spectrum). The PFE deposition time (2 min) for these experiments was chosen to obtain a continuous coating on the fibers with a thickness (∼100 nm) that is sufficient to retard water absorption into paper [48]. As a result, the fiber surface after a 2 min PFE deposition should have a Young CA approximately equal to 105°.

If the water–substrate interaction occurs in the ideal Cassie regime (Fig. 6a) with chemical heterogeneity provided by the PFE film and air, the minimum possible receding CA obtained would be ∼105° [6, 8]. However, in Fig. 4 we see that for 0 min etching, the receding CA values are well below 105°, as low as ∼10°. Such low receding CA values for these samples are only possible if pinning of the three phase contact line occurs by physical heterogeneities on the handsheet fibers. Since the wetting of handsheets seems to be in the Cassie regime (irrespective of the etching time), the high hysteresis could result only if there is a possibility of a nano-scale Wenzel state [3, 4] on the top of each fiber of the handsheet, characterized by an

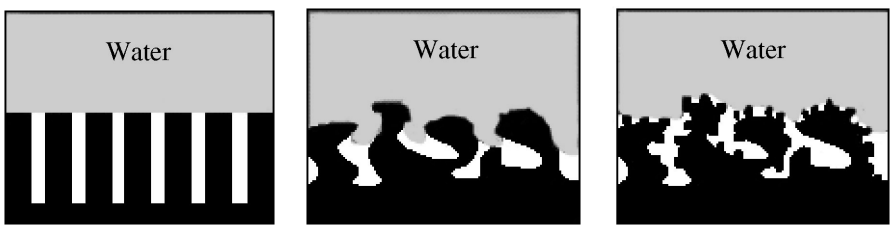

Figure 6. Schematics of interactions of water with surfaces at an ideal Cassie state (a), sticky superhydrophobic state (b) and roll-off superhydrophobic state (c).

enhanced liquid–substrate contact area (Fig. 6b). This type of interaction would increase the energy barrier between metastable states. For a surface with a very low solid–liquid contact area, a higher energy barrier greatly decreases the receding CA while only slightly increasing the advancing CA [8], as we observe for the handsheets. We believe that these types of interactions occur in the unetched handsheet with 2 min PFE deposition, resulting in a high, superhydrophobic advancing CA and a low, superhydrophilic receding CA. We categorize this type of interaction as Cassie state on the micro-scale and Wenzel state on the nano-scale. The unique combination of Cassie and Wenzel states provides a large energy barrier for the movement of the three phase contact line, resulting in a very low receding CA in spite of a superhydrophobic advancing CA. Similar types of interactions for different roughness scales are also referred to as 'air pocket trapping' [52], 'Cassie impregnation' [38, 53], 'petal effect' [38], 'transitional superhydrophobic state between Wenzel's and Cassie's states' [54] and 'Cassie–Wenzel wetting transition' [53, 55–59].

After etching, the formation of the nano-scale features on the fiber surface (see, e.g., 30 min in Fig. 5) provides a different liquid–solid interface. The additional roughness created by the nano-scale features results in Cassie state wetting at the nano-scale (Fig. 6c). We believe that these nano-scale features greatly reduce the wetting area, as well as the energy barrier between metastable states. As a result, the vibration energy of the drop is now high enough to overcome the energy barriers, giving rise to roll-off behavior (low CA hysteresis). We classify this type of interaction as Cassie regime on the nano- and micro-scale. This type of interaction is commonly referred to as the 'lotus state' [54], in reference to its natural occurrence on the leaves of lotus plants.

The schematics in Fig. 6b and 6c can be directly compared with the SEM images (Fig. 5a and 5b) for 0 and 60 min etched handsheets (HS-OD). Figure 4 shows that by varying the etching time, the hysteresis can be tuned from a sticky superhydrophobic to a roll-off superhydrophobic value. We believe that this tunability is obtained by a smooth transition from the Wenzel to Cassie state at the nano-scale (fiber surface) due to the evolution of the nano-scale features. This conclusion is supported by the SEM images in Fig. 5a and 5b (2 min PFE). The transition of a

drop's interaction from Cassie state to Wenzel state has been previously obtained by inducing pressure [60] and vibration [53, 55, 57–59]. Here, we obtain this transition without using an external stimulus by controlling the topography of the fibers or, in other words, by the evolution of the nano-scale features. In conclusion, the unique combination of transition in wetting happening at the nano-scale, while maintaining a Cassie state at the micro-scale results in variable receding CA while maintaining a superhydrophobic advancing CA.

3.6. Significance of Nano-scale Roughness on the Tunability of Stickiness

Fiber diameters in the handsheet range from 10 to 40 μm. Thus, a PFE film thickness of less than ∼1 μm would not be expected to affect the micro-scale roughness. Two PFE deposition times were used to coat the etched handsheets (2 and 15 min) to study the effect of nano-scale roughness on tunability. As explained previously, the 2 min PFE deposition (∼100 nm) was chosen because it just exceeds the minimum thickness to retard water absorption [48]. The 15 min PFE deposition (∼1 μm) was chosen because we believe this relatively thick film would not disturb the micro-scale features.

Comparisons of the advancing CA, receding CA and CA hysteresis for the 2 min and 15 min PFE-deposited handsheets (HS-OD) are shown in Fig. 4a and 4b. The 15 min PFE deposition on an unetched paper results in a CA hysteresis of $72.6 \pm 10^{\circ}$ which is lower than the value obtained for a 2 min PFE deposition. This observation is consistent with the SEM images in Fig. 5a. With increased PFE deposition (15 min), the presence of globular features is visible on the 0 min etched handsheets. We believe that these nano-scale features decrease the hysteresis by enhancing roughness. On the other hand, the CA hysteresis goes through a maximum value after 2 min etching and then decreases, following the same trend as the handsheets with 2 min PFE deposition. As explained previously, hysteresis increases with roughness if the interaction between the water drop and surface is in the Wenzel state. Hence, it can be concluded that 2 min etching increases the roughness scales (from 0 min etching) appropriate for Wenzel state wetting. After 3 min etching, the fiber topography is appropriate for wetting in the Cassie regime, resulting in a decrease in the CA hysteresis with respect to etching (roughness). It is evident from Fig. 4a and 4b that the hysteresis values for the etched fibers with 15 min of PFE deposition are consistently higher than for 2 min PFE deposition. This increased hysteresis may be attributed to the larger nano-scale features observed on handsheets after 15 min PFE deposition (Fig. 5a) which provide a larger solid–liquid contact area.

The morphological change on a nano-scale by longer deposition times (thicker PFE film) is a unique feature of the plasma deposition process. The plasma deposition process takes place at reduced pressure (∼1 Torr). At this pressure, the reactant species flux onto the surface, which establishes the deposition rate, is determined by the surface topography. That is, the film thickness at a particular surface location depends on the acceptance angle for species impingement and thus on the geometry

at that location [61]. Ideally, at the top of a 90° step, reactant flux impinges from a 270° cone and hence this edge location receives more flux than does a flat surface (180° cone) or the corner at the bottom of this step (90° cone); deposition rates scale with these fluxes. This phenomenon plays a crucial role in the modification of the oxygen etched fiber morphology due to the variation of PFE deposition thickness and deposition time.

Handsheets made with different fibers sizes were used to study the micrometer scale roughness on the wettability. The softwood fibers (3–7 mm in length; ∼50 μm in diameter) are typically larger than the hardwood fibers (1–2 mm in length; ∼20 μm in diameter) by a factor of two. Changing the micro-scale roughness by changing the fiber size combinations (100% hardwood (H), 100% softwood (S) and 50% hardwood–50% softwood (HS)) did not affect the CA or CA hysteresis values (data not shown). This clearly indicates that the physical heterogeneity (roughness) created on the fibers by oxygen etching is the key to tuning contact angle hysteresis and stickiness. This further strengths our hypothesis that nano-scale features created by oxygen etching are the key to the transition from a Wenzel-type wetting to a Cassie-type wetting at the nano-scale.

In Fig. 7, we have plotted the CA hysteresis and advancing CA for the different handsheets for the various etching times (0–60 min) with 2 min PFE deposition (HS-OD, H, S and HS) and with 15 min PFE deposition (HS-OD). This figure reiterates that all substrates (except two) are superhydrophobic by the classical definition (CA > 150°), but span a wide range of stickiness (CA hysteresis).

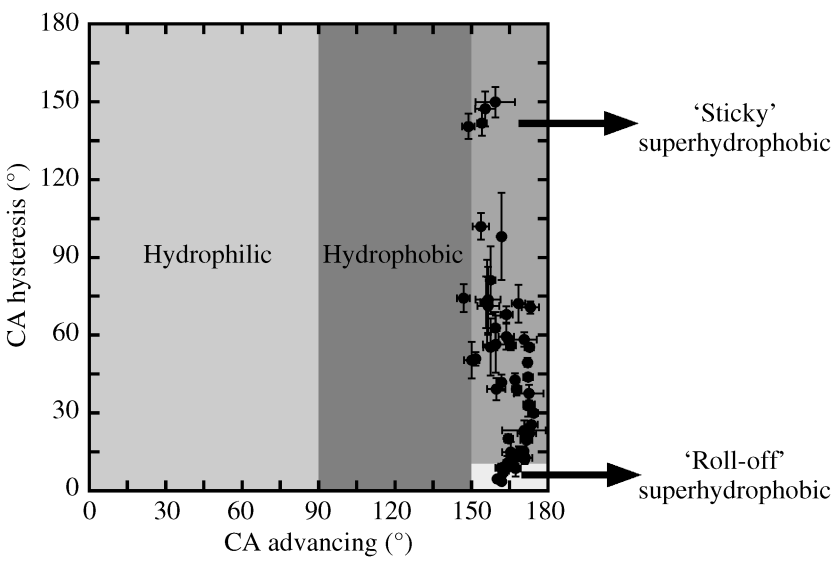

Figure 7. CA hysteresis *versus* CA for all samples investigated for various etching times: HS-OD, H, S and HS with 2 min PFE deposition and also HS-OD with 15 min PFE deposition.

4. Conclusions

We have reported the fabrication of superhydrophobic paper surfaces with a wide range of contact angle hysteresis values, which results in variable stickiness for water drops. The tunability of hysteresis on the paper substrates was obtained by creating physical heterogeneity (roughness) on the cellulose fibers *via* selective oxygen plasma etching. Tunable stickiness of water drops on paper-based substrates can be important in controlling the mobility of drops resident on the surface. Sticky superhydrophobic surfaces can also be a used to make 'tweezers' for liquid drops that allow the transfer of a large volume of liquid with low solid–liquid contact area. These concepts may open new windows of opportunities in many chemical and biomedical research areas such as microfluidics, MEMS, proteomics and genomics. In addition, generation of such tunable surface properties on biodegradable, inexpensive, recyclable paper substrates may widen the scope of possible applications.

Acknowledgements

The authors thank Dr. Ashwini Sinha (Praxair) for generously donating the PFE gas, Dr. Christine Kranz (Georgia Tech) for performing the FIB studies, Yonghao Xiu (Georgia Tech) for support with CA measurements, Dr. Gary Dobbs (ExxonMobil) for support with ATR–FT-IR measurements. B. B. thanks IPST for fellowship support.

References

1. T. Young, *Philosophical Trans. Royal Soc. London* **95**, 65–87 (1805).
2. R. E. Johnson, Jr. and R. H. Dettre, in: *Contact Angle, Wettability and Adhesion; Adv. Chem. Ser.*, R. F. Gould (Ed.), Vol. 43, pp. 112–135. Amer. Chem. Soc., Washington, DC (1964).
3. R. N. Wenzel, *Ind. Eng. Chem.* **28**, 988–994 (1936).
4. R. N. Wenzel, *J. Phys. Colloid Chem.* **53**, 1466–1467 (1949).
5. A. B. D. Cassie and S. Baxter, *Trans. Faraday Soc.* **40**, 546–550 (1944).
6. R. H. Dettre and R. E. Johnson, Jr., *J. Phys. Chem.* **69**, 1507–1515 (1965).
7. R. H. Dettre and R. E. Johnson, Jr., in: *Contact Angle, Wettability and Adhesion; Adv. Chem. Ser.*, R. F. Gould (Ed.), Vol. 43, pp. 136–144. Amer. Chem. Soc., Washington, DC (1964).
8. R. E. Johnson, Jr. and R. H. Dettre, *J. Phys. Chem.* **68**, 1744–1750 (1964).
9. A. M. Gaudin, A. F. Witt and T. G. Decker, *Trans. Soc. Mining Eng. AIME* **226**, 107–112 (1963).
10. W. Chen, A. Y. Fadeev, M. C. Hsieh, D. Oner, J. Youngblood and T. J. McCarthy, *Langmuir* **15**, 3395–3399 (1999).
11. D. Oner and T. J. McCarthy, *Langmuir* **16**, 7777–7782 (2000).
12. M. Morra, E. Occhiello and F. Garbassi, *Langmuir* **5**, 872–876 (1989).
13. J. P. Youngblood and T. J. McCarthy, *Macromolecules* **32**, 6800–6806 (1999).
14. M. Callies, Y. Chen, F. Marty, A. Pepin and D. Quere, *Microelectronic Eng.* **78**, 100–105 (2005).
15. J. L. Zhang, J. A. Li and Y. C. Han, *Macromol. Rapid Commun.* **25**, 1105–1108 (2004).
16. L. B. Zhu, Y. H. Xiu, J. W. Xu, P. A. Tamirisa, D. W. Hess and C. P. Wong, *Langmuir* **21**, 11208–11212 (2005).
17. K. Tadanaga, N. Katata and T. Minami, *J. Amer. Ceram. Soc.* **80**, 1040–1042 (1997).

18. A. Winkleman, G. Gotesman, A. Yoffe and R. Naaman, *Nano Lett.* **8**, 1241–1245 (2008).
19. J. D. Miller, S. Veeramasuneni, J. Drelich, M. R. Yalamanchili and G. Yamauchi, *Polym. Eng. Sci.* **36**, 1849–1855 (1996).
20. S. Veeramasuneni, J. Drelich, J. D. Miller and G. Yamauchi, *Prog. Org. Coat.* **31**, 265–270 (1997).
21. R. Di Mundo, F. Palumbo and R. d'Agostino, *Langmuir* **24**, 5044–5051 (2008).
22. Z. G. Guo and W. M. Liu, *Appl. Phys. Lett.* **90**, 223111–223113 (2007).
23. X. Hong, X. F. Gao and L. Jiang, *J. Amer. Chem. Soc.* **129**, 1478–1479 (2007).
24. M. H. Jin, X. J. Feng, L. Feng, T. L. Sun, J. Zhai, T. J. Li and L. Jiang, *Adv. Mater.* **17**, 1977–1981 (2005).
25. A. Hozumi and O. Takai, *Thin Solid Films* **303**, 222–225 (1997).
26. T. Onda, S. Shibuichi, N. Satoh and K. Tsujii, *Langmuir* **12**, 2125–2127 (1996).
27. S. Shibuichi, T. Onda, N. Satoh and K. Tsujii, *J. Phys. Chem.* **100**, 19512–19517 (1996).
28. Y. Kunugi, T. Nonaku, Y. B. Chong and N. Watanabe, *J. Electroanal. Chem.* **353**, 209–215 (1993).
29. K. Ogawa, M. Soga, Y. Takada and I. Nakayama, *Japanese J. Appl. Phys. Part 2 — Letters* **32**, L614–L615 (1993).
30. J. M. Schakenraad, I. Stokroos, H. Bartels and H. J. Busscher, *Cells Mater.* **2**, 193–199 (1992).
31. P. Roach, N. J. Shirtcliffe and M. I. Newton, *Soft Matter* **4**, 224–240 (2008).
32. B. Balu, V. Breedveld and D. W. Hess, *Langmuir* **24**, 4785–4790 (2008).
33. Y. Yao, X. Dong, S. Hong, H. Ge and C. C. Han, *Macromol. Rapid Commun.* **27**, 1627–1631 (2006).
34. D. Quere, M. J. Azzopardi and L. Delattre, *Langmuir* **14**, 2213–2216 (1998).
35. K. S. Liao, A. Wan, J. D. Batteas and D. E. Bergbreiter, *Langmuir* **24**, 4245–4253 (2008).
36. Y. B. Li, M. J. Zheng, L. Ma, M. Zhong and W. Z. Shen, *Inorganic Chem.* **47**, 3140–3143 (2008).
37. S. Boduroglu, M. Cetinkaya, W. J. Dressick, A. Singh and M. C. Demirel, *Langmuir* **23**, 11391–11395 (2007).
38. L. Feng, Y. Zhang, J. Xi, Y. Zhu, N. Wang, F. Xia and L. Jiang, *Langmuir* **24**, 4114–4119 (2008).
39. E. B. Dussan V. and R. T. P. Chow, *J. Fluid Mech.* **137**, 1–29 (1983).
40. E. B. Dussan V., *J. Fluid Mech.* **174**, 381–397 (1987).
41. E. B. Dussan V., *J. Fluid Mech.* **151**, 1–20 (1985).
42. M. Callies and D. Quere, *Soft Matter* **1**, 55–61 (2005).
43. S. Agraharam, D. W. Hess, P. A. Kohl and S. A. B. Allen, *J. Vac. Sci. Technol. A* **17**, 3265–3271 (1999).
44. G. T. Dobbs, B. Balu, C. Young, C. Kranz, D. W. Hess and B. Mizaikoff, *Anal. Chem.* **79**, 9566–9571 (2007).
45. O. L. Sponsler, *Ind. Eng. Chem.* **20**, 1060–1062 (1928).
46. W. H. Walker, *J. Franklin Institute* **164**, 131–140 (1907).
47. S. Sapieha, A. M. Wrobel and M. R. Wertheimer, *Plasma Chem. Plasma Proc.* **8**, 331–346 (1988).
48. S. Vaswani, J. Koskinen and D. W. Hess, *Surface Coatings Technol.* **195**, 121–129 (2005).
49. F. Ferrero and R. Bongiovanni, *Surface Coatings Technol.* **200**, 4770–4776 (2006).
50. S. Y. Oh, D. I. Yoo, Y. Shin and G. Seo, *Carbohydrate Res.* **340**, 417–428 (2005).
51. S. M. Mukhopadhyay, P. Joshi, S. Datta, J. G. Zhao and P. France, *J. Phys. D — Appl. Phys.* **35**, 1927–1933 (2002).
52. P. G. de Gennes, F. Brochard-Wyart and D. Quéré, *Capillarity and Wetting Phenomena: Drops, Bubbles, Pearls, Waves.* Springer, New York, NY (2003).
53. E. Bormashenko, R. Pogreb, G. Whyman, Y. Bormashenko and M. Erlich, *Appl. Phys. Lett.* **90**, 201917-1–20917-2 (2007).
54. S. Wang and L. Jiang, *Adv. Mater.* **19**, 3423–3424 (2007).

55. E. Bormashenko, Y. Bormashenko, T. Stein and G. Whyman, *J. Colloid Interface Sci.* **311**, 212–216 (2007).
56. E. Bormashenko, Y. Bormashenko, T. Stein, G. Whyman and R. Pogreb, *Langmuir* **23**, 4378–4382 (2007).
57. E. Bormashenko, R. Pogreb, T. Stein, G. Whyman, M. Erlich, A. Musin, V. Machavarianib and D. Aurbach, *Phys. Chem. Chem. Phys.* **10**, 4056–4061 (2008).
58. E. Bormashenko, R. Pogreb, G. Whyman and M. Erlich, *Langmuir* **23**, 6501–6503 (2007).
59. E. Bormashenko, R. Pogreb, G. Whyman and M. Erlich, *Langmuir* **23**, 12217–12221 (2007).
60. A. Lafuma and D. Quere, *Nature Mater.* **2**, 457–460 (2003).
61. B. L. Chin and E. P. Van de Ven, *Solid State Technol.* **31**, 119–122 (1988).